Three-Dimensional, Transient, Saturated–Unsaturated Flow in a Groundwater Basin

R. ALLAN FREEZE

IBM Thomas J. Watson Research Center, Yorktown Heights, New York 10598

Abstract. A three-dimensional finite difference model has been developed for the treatment of saturated–unsaturated transient flow in small nonhomogeneous, anisotropic geologic basins. The uniqueness of the model lies in its inclusion of the unsaturated zone in a basin wide model that can also handle both confined and unconfined saturated aquifers, under both natural and developed conditions. The integrated equation of flow is solved by the line successive overrelaxation technique. The model allows any generalized region shape and any configuration of time variant boundary conditions. When applied to natural flow systems, the model provides quantitative hydrographs of surface infiltration, groundwater recharge, water table depth, and stream base flow. Results of simulations for hypothetical basins provide insight into the mechanisms involved in the development of perched water tables. The unsaturated basin response is identified as the controlling factor in determining the nature of the base flow hydrograph. Application of the model to developed basins allows one to simulate not only the manner in which groundwater withdrawals are transmitted through the aquifers, but also the changes in the rates of groundwater recharge and discharge induced by the withdrawals. For any proposed pumping pattern, it is possible to predict the maximum basin yield that can be sustained by a flow system in equilibrium with the recharge–discharge characteristics of the basin.

INTRODUCTION

The requirements of water resource planning have made simulation of the hydrologic response of groundwater basins a technique of increasing importance. In this paper a numerical mathematical model is presented that attempts to bring the state of the science one step closer to hydrogeologic reality. The uniqueness of the model is shown in the following general set of properties:

1. The model is three-dimensional. It can also collapse to treat two-dimensional vertical cross sections.
2. The model has its upper boundary at the ground surface. It treats the complete subsurface regime as a unified whole because the flow in the unsaturated zone is integrated with saturated flow in the underlying unconfined and confined aquifers.
3. The model is a transient analysis. It can handle both the natural transient boundary conditions that occur at the ground surface and the man-made transient effects created by aquifer development. It can also treat steady state systems.
4. The model allows consideration of nonhomogeneous and anistropic geologic formations.
5. The model admits any generalized configuration of all pertinent boundary conditions.

Ultimately, it is planned to incorporate this model into a complete hydrologic response model of the type espoused by *Freeze and Harlan* [1969]. However, in this paper I will treat only the more classic application to problems in basin hydrogeology.

Transient numerical models that integrate the saturated and unsaturated zones were pioneered by *Rubin* [1968]. His paper was followed by several other two-dimensional applications to various specific problems [*Hornberger et al.*, 1969; *Taylor and Luthin*, 1969; *Verma and Brutsaert*, 1970]. These studies used Laplace's equation in the saturated zone and are thus limited to near-surface flow in homogeneous, incompressible, and unconfined aquifers. *Cooley* [1970] studied pumping from an aquifer system by using a form of the complete equations. All these studies were for regions of limited size with specialized boundary configurations. Only *Jeppson* [1969] has considered the sat-

urated–unsaturated flow regime on a basin wide scale, but he restricted himself to a steady state treatment.

In this paper, following some comments on terminology, there are three mathematical sections: (1) equation of flow, (2) numerical method of solution, and (3) limitations of the present model. These three sections are followed by some hydrogeologic simulations of hypothetical basins. Infiltration, groundwater recharge, and stream base flow are discussed on the basis of some two-dimensional vertical simulations of natural flow systems; and a three-dimensional simulation of a developed basin is used as the basis for a discussion of the concepts of basin yield.

SOME COMMENTS ON TERMINOLOGY

There are several sets of concepts and terms common in groundwater hydrology that lose their significance when the treatment is three-dimensional or when consideration of the unsaturated zone is included.

The coefficients of transmissibility and storage do not appear in this paper. They are two-dimensional concepts, well suited to the development of aquifer oriented, pump testing treatments but meaningless in three-dimensional flow simulations. The more fundamental parameters of specific permeability, porosity, and the compressibilities of water and soil are used throughout this paper.

The concept of specific yield is outmoded when continuous flow between the saturated and unsaturated zones is considered. It should also be noted that the integrated analysis dispenses with the need for complex 'free surface' computations, or the invocation of Dupuit-Forscheimer assumptions, or assumptions that limit the saturated thickness of unconfined aquifers.

In the unsaturated zone, descriptive terms such as wilting point and field capacity are outdated. There does not appear to be any advantage to using the concept of infiltration capacity rather than the more fundamental parameters to which it is related such as the saturated permeability of the soil.

I have already used the terms 'unconfined' and 'confined' when referring to groundwater aquifers, but they are used here only in a descriptive sense. The limitations and specialized boundary conditions inherent in their usage in the pump testing literature do not apply to this model.

EQUATION OF FLOW

It is necessary to develop an equation of flow that will hold for saturated flow in both confined and unconfined aquifers and for flow in the unsaturated zone. The unsaturated zone actually involves a two-phase flow of air and water and thus could be treated by the techniques developed for multiple phase flow in the petroleum industry. Such an approach was outlined by *Nelson* [1966] and has recently been carried out by *Green et al.* [1970]. The main disadvantage to following such a course at this time for large basin oriented models is the computational complexity that is added to the problem.

The alternative approach used in this study employs a single equation that considers only the flow of water. The fundamental assumption is that the air phase is continuous and is at atmospheric pressure. This assumption precludes the entrapment of pockets of compressible air in the flow system. This assumption could prove to be a serious limitation in some applications, but it has been universally used by soil physicists in the solution of irrigation and drainage problems without misgivings and with apparent success.

The equation is best presented as a combination of the saturated equation developed by *Jacob* [1940] and clarified by *Cooper* [1966] and the unsaturated equation of *Richards* [1931]. I have written the equation in terms of the pressure head $\psi = \psi\ (x, y, z, t)$, where $\psi > 0$ implies saturated conditions and $\psi < 0$ implies unsaturated conditions. The pressure p is related to ψ by the familiar relation $p = \rho g \psi$. In the cgs system, the units of ψ are cm of water. The sum of the pressure head ψ and the elevation head z is the total hydraulic head ϕ.

To be perfectly general, the equation should be developed in deforming coordinates, the Darcy velocity being considered as a relative velocity of the water with respect to the grains [*Cooper*, 1966]. The equation presented here is derived following these considerations, but in the computer applications that follow the coordinates are taken as fixed. This is a standard approximation that apparently leads to little error. It is also possible to view the equation as

having been developed in fixed coordinates. In this case, the approximation takes the form of discarding terms in which the velocity of the soil grains is multiplied by the vertical pressure head gradient. These are the only terms that are dropped from this development.

The Darcy velocity can be formulated as

$$\mathbf{v}_d = Sn(\mathbf{v}_w - \mathbf{v}_s) = -\frac{g\rho k}{\mu}(\nabla\psi + \nabla z) \qquad (1)$$

where $\mathbf{v}_d$, the relative velocity of water with respect to the soil, is equal to (v_{dx}, v_{dy}, v_{dz}); $\mathbf{v}_w$, the velocity of water, is equal to (v_{wx}, v_{wy}, v_{wz}); $\mathbf{v}_s$, the velocity of soil grains, is equal to $(0, 0, v_{sz})$; and the rest of the standard terms are listed with their cgs units in the notation. It should be noted that

$$\rho = \rho(\psi) \qquad (2a)$$

$$k = k(F, \psi) = k_{ii} \qquad (2b)$$

where k_{ii} are the principal components of (k_{ij}),

$$n = n(F, \psi) \qquad (2c)$$

$$\theta = \theta(F, \psi) = Sn \qquad (2d)$$

In saturated regions, the specific permeability k is a function of position owing to the nonhomogeneity of the geologic formations $F = F(x, y, z)$. In unsaturated regions k is a function of position and time even in homogeneous soils, owing to the variation of k with ψ. Equation 2*d* relates the moisture content θ to the fractional saturation S and to the porosity n.

The equation of continuity for water is

$$-\nabla\cdot(Sn\rho\mathbf{v}_w) = \frac{\partial}{\partial t}(Sn\rho) \qquad (3)$$

where

$$\rho = \rho_0 \exp(\beta'\psi) \qquad (4)$$

and

$$\beta' = \beta\rho g \qquad (5)$$

β being the usual coefficient of water compressibility. The equation of continuity for the soil is

$$-\nabla\cdot[(1 - n)\rho_s\mathbf{v}_s] = \frac{\partial}{\partial t}[(1 - n)\rho_s] \qquad (6)$$

Following an approach similar to *Verruijt's* [1969] very elegant development of the saturated equation, one can develop an integrated equation by combining equations 1, 3, and 6 to give

$$\nabla\cdot\left[\frac{\rho^2 gk}{\mu}(\nabla\psi + \nabla z)\right] = [S\rho(\alpha' + n\beta') + \rho C]\frac{\partial\psi}{\partial t}$$

where

$$C = C(F, \psi) = n\frac{\partial S}{\partial\psi} = \frac{\partial\theta}{\partial\psi}$$

and $\alpha' = \alpha\rho g$, α being the usual coefficient of vertical formation compressibility. C is the specific moisture capacity.

Expanding and noting (2) we have the final equation of flow

$$\frac{\partial}{\partial x}\left[\frac{g}{\mu}\rho^2(\psi)k_{xx}(F, \psi)\frac{\partial\psi}{\partial x}\right] + \frac{\partial}{\partial y}\left[\frac{g}{\mu}\rho^2(\psi)k_{yy}(F, \psi)\frac{\partial\psi}{\partial y}\right] + \frac{\partial}{\partial z}\left[\frac{g}{\mu}\rho^2(\psi)k_{zz}(F, \psi)\left\{\frac{\partial\psi}{\partial z} + 1\right\}\right] = \left[\frac{\rho(\psi)\theta(F, \psi)}{n(F, \psi)}\{\alpha'(F) + n(F, \psi)\beta'(F)\} + \rho(\psi)C(F, \psi)\right]\frac{\partial\psi}{\partial t} \qquad (7)$$

By leaving the ρ and k terms inside the outer spatial derivatives, we maintain in the solution the effects of spatial changes in density and all the higher order derivatives that are often discarded. It is not permissible to cancel the ρ term from the left- and right-hand sides.

Equation 7 must be viewed relative to the basic functional inputs $\rho(\psi)$, $k(\psi)$, $\theta(\psi)$, and $n(\psi)$ and the parameters α', β', and $C(\psi)$, which are developed from them. Figure 1 is a schematic diagram that shows these relations. The density of water follows the expression given in equation 4 and shown in Figure 1*a*. This relation also defines the compressibility of water β'. β' is actually a function of ψ because of the ρ on the right-hand side of (5), but there is negligible error in defining $\beta' = \beta\rho_0 g$, whereby β' has a constant value as shown in the right-hand diagram of Figure 1*a*. It should be noted

that there is no discontinuity in the value of the compressibility as ψ changes from positive saturated pressure heads to negative unsaturated pressure heads [*Dorsey*, 1940, p. 241].

The hysteretic functional relationship between specific permeability and pressure head is shown in Figure 1*b*. There is actually an infinite number of scanning curves s between the bounding drying curve d and the wetting curve w, but only one is shown. For $\psi > 0$, k is usually taken as a constant (solid line), but the increase in k due to the increase in porosity (broken line) may be included. *Madsen* [1969] has suggested that this increase in permeability can be of considerable importance.

Laboratory measurements are usually presented as K–ψ curves where K is hydraulic conductivity. These curves can easily be converted to k–ψ by the well-known relationship $k = K\mu/\rho g$.

Figure 1*c* shows the moisture content relationship θ–ψ. The saturated moisture content equals the porosity. Again, the broken line shows the optional possibility of considering the increase in porosity with increased positive pressure head. The slope of the θ–ψ curve is defined as the specific moisture capacity $C(\psi)$. The nature of this function is shown in the right-hand diagram of Figure 1*c*.

For those soils in which saturation is achieved at a pressure head slightly less than zero (the air entry pressure head), the curves of Figures 1*b* and 1*c* would be displaced slightly to the left. In such soils, a tension saturated zone (the capillary fringe) occurs above the water table.

The vertical compressibility of the soil is defined by a series of equalities relating the pore volume and the soil stresses. The complete set of equalities [*Verruijt*, 1969] is

$$\frac{\partial v_{ss}}{\partial z} = \frac{\partial e}{\partial t} = \frac{\partial \epsilon_s}{\partial t} = -\alpha \frac{\partial \sigma_s}{\partial t} = \alpha \frac{\partial p}{\partial t} = \alpha' \frac{\partial \psi}{\partial t} \qquad (8)$$

where e is volume strain, ϵ_s is vertical strain, and σ_s is effective vertical stress. From the second and sixth members of (8) one can derive $dn/(1 - n) = \alpha' d\psi$, which is the fundamental relation shown in Figure 1*d*. The vertical aquifer compressibility is a step function, as shown in the right-hand diagram of Figure 1*d*.

The relationships of (8) are valid for confined elastic aquifers. Their relevance to unconfined and unsaturated aquifers must be investigated. The equality between the fourth and fifth terms in (8) is based on the assumption that a change in pore pressure must immediately produce an equal and opposite change in effective stress, owing to the constant weight per unit area of the overlying column of solids and fluids. In the unconfined zone it no longer seems reasonable to assume the constancy of overlying weight. Changes in the overlying fluid content may create load changes that are a significant percentage of the total load. In the unsaturated zone, there are still changes in the overlying load, but presumably the pore 'tension' has no ability to support the load.

If one follows these considerations through, it is possible to derive a new α' term to be added to the right-hand side of the equation of flow (equation 7). My conclusion, however, is that such a term is numerically insignificant. For natural flow systems, α' and β' are both negligible in their effects on the flow patterns. For pumped flow systems, the effects of changes in ψ should overshadow the effects of changes in overlying θ.

NUMERICAL SOLUTION

The equation of flow (7) is a nonlinear parabolic partial differential equation. An iterative numerical scheme that uses implicit finite difference formulations should minimize the computer time for its solution and will also guarantee unconditional stability for all size time steps (although the accuracy will be decreased by the use of larger time steps). Iterative techniques have an added advantage over direct techniques for our problem in that they allow for recalculation at each iteration of the terms that are functions of the dependent variable.

There are three implicit iterative methods that can be considered: the line successive overrelaxation (LSOR) technique [*Young*, 1962], the iterative variant [*Wachpress and Habetler*, 1960] of *Douglas and Rachford*'s [1956] alternating direction implicit procedure (ADIPIT), and the strongly implicit procedure (SIP) of *Stone* [1968]. Papers from the petroleum industry comparing these techniques for two-dimensional reservoir analyses [*Briggs and*

Dixon, 1968; *Bjordammen,* 1969; *Weinstein et al.,* 1969] show that each technique can be proved superior for certain cases. Differences in the total computing time rarely exceed a factor of 2 and are usually within 10–25%. For a saturated–unsaturated flow problem, *Cooley* [1970] concluded that although the ADIPIT and LSOR methods produced satisfactory results, the LSOR technique was faster and easier to use.

In this study the LSOR technique, oriented in the z direction, was used with a block centered nodal grid (Figure 2). The mesh spacings can be variable, and the region can be of any general shape that does not lead to a discontinuity in any of the vertical nodal columns. For an interior node (subscripts i, j, k) at time step t (superscript t), the finite difference approximation to (13) is

$$\begin{aligned}
&\left\{\frac{g}{\mu\Delta x_i}\left[\rho^2(\psi_{\mathrm{I}})k(\psi_{\mathrm{I}})\left(\frac{1}{\Delta x_i+\Delta x_{i+1}}(\psi_{i+1}{}^{t}+\psi_{i+1}{}^{t-1}-\psi_i{}^{t}-\psi_i{}^{t-1})\right)\right.\right.\\
&\qquad\left.\left.-\rho^2(\psi_{\mathrm{II}})k(\psi_{\mathrm{II}})\left(\frac{1}{\Delta x_i+\Delta x_{i-1}}(\psi_i{}^{t}+\psi_i{}^{t-1}-\psi_{i-1}{}^{t}-\psi_{i-1}{}^{t-1})\right)\right]\right\}_{j,k}\\
&\quad+\left\{\frac{g}{\mu\Delta y_j}\left[\rho^2(\psi_{\mathrm{III}})k(\psi_{\mathrm{III}})\left(\frac{1}{\Delta y_j+\Delta y_{j+1}}(\psi_{j+1}{}^{t}+\psi_{j+1}{}^{t-1}-\psi_j{}^{t}-\psi_j{}^{t-1})\right)\right.\right.\\
&\qquad\left.\left.-\rho^2(\psi_{\mathrm{IV}})k(\psi_{\mathrm{IV}})\left(\frac{1}{\Delta y_j+\Delta y_{j-1}}(\psi_j{}^{t}+\psi_j{}^{t-1}-\psi_{j-1}{}^{t}-\psi_{j-1}{}^{t-1})\right)\right]\right\}_{i,k}\\
&\quad+\left\{\frac{g}{\mu\Delta z_k}\left[\rho^2(\psi_{\mathrm{V}})k(\psi_{\mathrm{V}})\left(1+\frac{1}{\Delta z_k+\Delta z_{k+1}}(\psi_{k+1}{}^{t}+\psi_{k+1}{}^{t-1}-\psi_k{}^{t}-\psi_k{}^{t-1})\right)\right.\right.\\
&\qquad\left.\left.-\rho^2(\psi_{\mathrm{VI}})k(\psi_{\mathrm{VI}})\left(1+\frac{1}{\Delta z_k+\Delta z_{k-1}}(\psi_k{}^{t}+\psi_k{}^{t-1}-\psi_{k-1}{}^{t}-\psi_{k-1}{}^{t-1})\right)\right]\right\}_{i,j}\\
&=\left\{\left[\frac{\rho(\psi_{\mathrm{VII}})\theta(\psi_{\mathrm{VII}})}{n(\psi_{\mathrm{VII}})}(\alpha'+n(\psi_{\mathrm{VII}})\beta')+\rho(\psi_{\mathrm{VII}})C(\psi_{\mathrm{VII}})\right]\left(\frac{\psi^t-\psi^{t-1}}{\Delta t^t}\right)\right\}_{i,j,k} \qquad (9)
\end{aligned}$$

For vertical LSOR, the terms can be grouped as

$$-A_k\psi_{i,j,k+1}{}^{t}+B_k\psi_{i,j,k}{}^{t}-C_k\psi_{i,j,k-1}{}^{t}=D_k \qquad (10)$$

where A_k, B_k, C_k, and D_k are developed from the groupings of the coefficients of (9). During the scanning of each line in the three-dimensional mesh, values of ψ^t on adjacent lines, as calculated from the most recent iteration, are considered as known values, as all values of ψ^{t-1} are. The set of equations (10) for a line scan, form a tridiagonal matrix equation that can be solved by the well-known triangularization scheme used in both the ADIPIT and LSOR procedures. After each iteration (superscript it) the calculated values of ψ at each node are overrelaxed in the usual fashion

$$\psi^{t,it}=\omega\psi_{\mathrm{calc}}{}^{t,it}+(1-\omega)\psi^{t,it-1} \qquad 1\le\omega\le 2$$

At each iteration it is necessary to predict a pressure head value $\psi_{(\mathrm{pred})}$ at each node, from which the current estimates of ρ, k, θ, n, and C can be calculated. For the first iteration of the first time step

$$\psi_{(\mathrm{pred})i,j,k}{}^{t}=\psi_{i,j,k}{}^{t-1} \qquad (11)$$

where $t=0$ implies initial conditions. For the first iteration of later time steps

$$\psi_{(\mathrm{pred})i,j,k}{}^{t}=(T_t+1)\psi_{i,j,k}{}^{t-1}-T_t\psi_{i,j,k}{}^{t-2} \qquad (12)$$

where

$$T_t=\frac{\Delta t^t}{2\,\Delta t^{t-1}}$$

For later iterations of all time steps [*Cooley,* 1970]

$$\psi_{(\mathrm{pred})i,j,k}{}^{t,it}=\psi_{(\mathrm{pred})i,j,k}{}^{t,it-1}+\lambda(\psi_{i,j,k}{}^{t,it-1}-\psi_{(\mathrm{pred})i,j,k}{}^{t,it-1}) \qquad 0\le\lambda\le 1 \qquad (13)$$

The value of ψ_{I} that appears in equation 17 is

the predicted value of ψ at the boundary between two nodal blocks (Figure 2). It is determined by

$$\psi_{\mathrm{I}} = \tfrac{1}{2}(\psi_{(\mathrm{pred})i,j,k} + \psi_{(\mathrm{pred})i+1,j,k})$$

The values of ψ_{II} through ψ_{VI} are determined analogously. ψ_{VII} is equal to $\psi_{(\mathrm{pred})i,j,k}$. If the nodal boundary at which ψ_{I} is calculated is also a geologic boundary between formations or soils of permeability k_1 and k_2, then

$$k(\psi_{\mathrm{I}}) = \tfrac{1}{2}[k_1(\psi_{\mathrm{I}}) + k_2(\psi_{\mathrm{I}})]$$

For steady state flow (which was often set up as the initial condition), the optimum value of the overrelaxation parameter ω was found to be 1.88. When equation 12 was used as the initial predictor for later time steps, it replaced the need for overrelaxation, and a relaxation parameter of $\omega = 1.00$ was used. I also tried using equation 11 in conjunction with equation 13 for later time steps, using an ω value of 1.30 [*Cooley*, 1970]. These combinations define two methods of obtaining convergence: (1) equations 11 and 13 with $\omega = 1.30$, and (2) equations 12 and 13 with $\omega = 1.00$. Operationally, it was found that there was little to choose between the two methods, both generally giving rise to convergence to a tolerance of 0.001 within 10 iterations. Attempts to mix the two techniques, however, led to divergence. I made no attempt to optimize λ, since solution times did not appear to be very sensitive to this parameter.

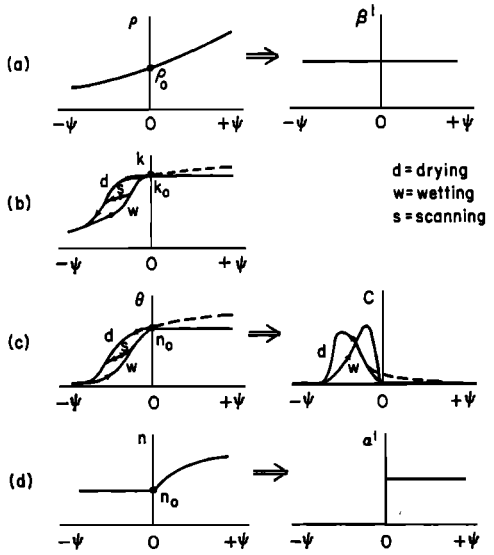

Fig. 1. Schematic diagram of the functional inputs. (*a*) Density of water $\rho(\psi)$ and compressibility of water β'. (*b*) Specific permeability of the soil $k(\psi)$. (*c*) Moisture content $\theta(\psi)$ and specific moisture capacity $C(\psi)$. (*d*) Porosity $n(\psi)$ and vertical compressibility of the soil α'.

At any boundary node, boundary conditions can be imposed that specify the flux, the head, or no-flow conditions. For flux across the upper z boundary of a nodal block, the first term in the finite difference representation of flow in the z direction in equation 9 is replaced by $[\rho\ (\psi_{\mathrm{VII}})\ I_s]/\Delta z$, where I_s positive is an inflow rate and I_s negative is an outflow rate. Similar expressions hold for the six possible locations of flux into or out of any given node. For a no-flow boundary, $I = 0$.

The application of a specified head boundary condition at the nodal point rather than at the nodal block boundary (Figure 2) gives rise to slight discontinuities along mixed boundaries, but these are smoothed out within one node of the boundary.

It is also possible to simulate an internal source or sink representing a recharge or pumping well. The node containing the well itself is considered to be outside the model, and the six surrounding nodal blocks are treated with the appropriate side as a flux boundary. Such an approach is not intended to provide exact duplication of flow conditions near the well. Rather, the emphasis is on the effect on a regional scale. It is also possible to represent an internal source or sink by a constant head node rather than by the above approach, which duplicates constant discharge conditions.

The program has been written to allow timewise variations in the flux rates along boundaries, but for the examples presented in this paper the specified flux rates are kept constant throughout the runs. The possible numerical complications that may be induced by time dependent boundary fluxes have therefore not been exposed. In the figures, all the simulated rainfall rates are less than the surface saturated hydraulic conductivities, but cases were simulated that involved surface ponding and surface saturation. When ponding occurs, the upper boundary condition changes from a specified flux to a specified ponding head. It is also necessary

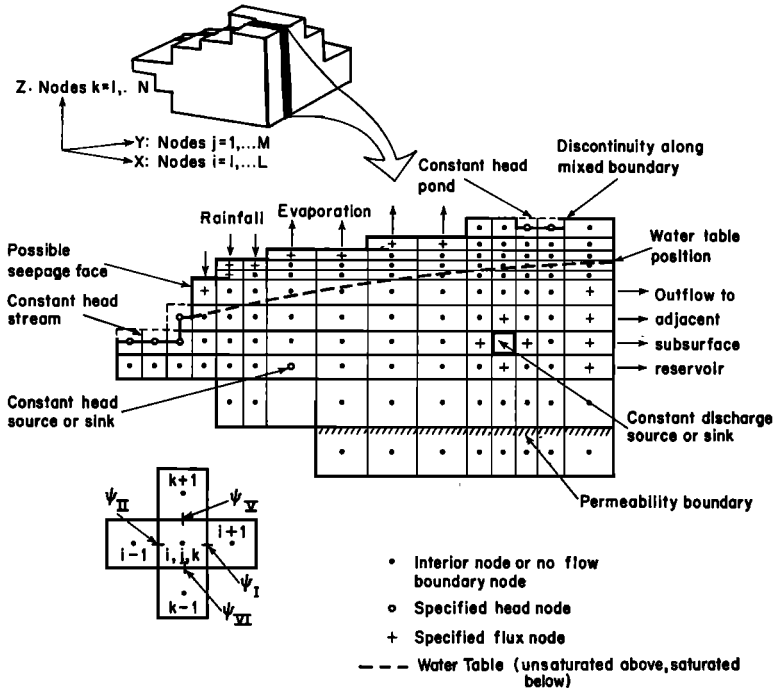

Fig. 2. Block centered nodal grid used in LSOR numerical solution. Possible boundary conditions are shown schematically. Lower inset defines ψ_I–ψ_{VI} values used in finite difference equations.

to allow boundary conditions to change from one boundary type to another during the course of a solution that involves a seepage face. The face is a no-flow boundary as long as $\psi < 0$ but becomes a constant head boundary, allowing outflow, once ψ attains the value $\psi = 0$. The programing complications engendered by rising and falling seepage faces in a saturated–unsaturated analysis will not be discussed further here.

The functional relationships shown in Figures 1*b* and 1*c* are built into the computer program as a table of values representing the wetting, drying, and scanning curves of the hysteretic relationships. This table of values is a line segment representation with linear interpolation between the coordinate points. In this study, 12 line segments were used for each curve, and seven scanning curves were used for each soil. The program locates the correct curve after determining whether the node in question is wetting or drying by scanning the past history of the node to determine the pressure head value at which a change from wetting to drying, or vice versa, occurred. For those geologic formations that occur at depth, it is usually only necessary to use saturated data.

The time step size may also be varied in several ways, so that one can choose a series of time steps suited to the particular problem being solved.

Output is in the form of plots of the pressure head, total head, and moisture content fields for any desired cross section at any desired time step. From the pressure head diagram one can locate the position of the water table. From the total head diagram one can determine the flow pattern and quantitative values of the infiltration rate, recharge rate, and base flow rate.

The program has been written so that it can collapse from three dimensions to two and from a transient analysis to steady state.

The program language is Fortran IV. Computer runs were carried out at the Thomas J. Watson Research Center on an IBM System 360 model 91 computer with 1.5×10^6 bytes of available core storage. A Stromberg-Datagraphix

model SC 4020 photographic plotter made rapid plotting easier.

ASSUMPTIONS AND LIMITATIONS

Despite the considerable effort that was expended in this study to develop a versatile mathematical model with a wide range of applications, it is still necessary to emphasize the theoretical assumptions on which the model is based and the limitations that are imposed on its use by the present generation of computers.

The mathematical development is based on the usual set of assumptions for saturated flow; namely, that the flow is laminar and Darcian and that inertial forces, velocity heads, temperature gradients, osmotic gradients, and chemical concentration gradients are all negligible. The soils and geologic formations are assumed to be linearly and reversibly elastic and mechanically isotropic; horizontal components of deformation are assumed small compared to vertical deformations. The analysis requires that the velocity of the soil grains be negligible and that the principal directions of anisotropy parallel the coordinate directions. In the unsaturated zone, it is assumed that the soils are nonswelling and that the air phase is continuous and always in connection with constant external atmospheric pressure.

Many of these assumptions are not restrictive, but there are three critical ones that limit the sphere of application. These are the two unsaturated assumptions that disallow entrapped air and swelling soils, and the temperature gradient restriction that precludes treatment of winter soil moisture conditions in northern latitudes. If subsurface flow models are to play a useful role in overall watershed response models, it may be necessary to integrate recent work by soil physicists in these fields to obtain sufficient generality.

With my program, the IBM 360/91 could accommodate a mesh of 30,000 nodes. This figure was adequate for two-dimensional cross sections but still placed a limitation on the study of basin wide hydraulics in three dimensions (to nets of, say, $20 \times 30 \times 50$). At surface boundary nodes where flux enters or leaves the system, it is necessary to have small vertical nodal spacings of the order of 10–100 cm for most realistic cases. A close nodal spacing is also necessary in the vicinity of wells and streams. Even with large horizontal nodal spacings and nets that widen quickly about these critical zones, the size of a basin that can be modeled entirely within core is limited to a few square miles by 1000 feet deep.

With rapid access external storage, much larger models can be accommodated but at the expense of computer times that would probably become excessive.

Despite the stability of the LSOR numerical scheme, a time step limitation is introduced by the nonlinearity of the coefficients. For the flow systems simulated in this study, it was found that pressure head changes should not exceed about 10 cm at any node during a time step. For early stages of well pumping, this may mean an initial time step as small as 0.01 second. For low rate natural infiltration, time steps of a day or even a week may be permissible. Where small initial time steps are needed, it is permissible to increase the step with time by using a rapid geometric progression. For most hydrologic events, it is usually possible to chart the main response within 10–200 time steps. On the model 91, a 200 time step solution to a 50×50 two-dimensional model takes 5–10 minutes of computer time.

Many authors [e.g., *Verma and Brutsaert*, 1970] have reported difficulties in obtaining convergence when solving parabolic equations in which the coefficients are functions of the dependent variable. This study was not immune to such problems. The failure usually takes the form of an oscillation of predicted and calculated ψ about the correct value, so that the solution fails to converge to the desired tolerance. In rare cases converging solutions actually did a turnabout and began diverging. I found no magic solutions, but I did have moderate success with a mechanism built into the program, whereby the time step size was automatically reduced by a specified factor and the step recalculated when such problems occurred.

Complex models are open to the charge that their sophistication outruns the available data. For example, this model can use (although it does not require) anisotropy values. Such data are only rarely available in the saturated zone, and the concept is completely disregarded in most studies of the unsaturated zone. The hysteretic relationships that make up the hydrologic properties of the soil also constitute data

that are in short supply. To answer the charge, one can only reply that the deterministic simulation approach espoused here is potentially superior to any empirical technique that requires less data. If the technique can be shown to have practical value, it will encourage increased measurement of the necessary data.

INFILTRATION AND GROUNDWATER RECHARGE

The interrelationship between infiltration and groundwater recharge has been studied in one dimension by *Freeze* [1969]. The parameters identified there controlling the natural replenishment of groundwater basins are also operative in two and three dimensions. These parameters are the rate and duration of rainfall, the climatic conditions during the subsequent redistribution period, the rate and direction of groundwater flow at the water table (groundwater recharge rate), the antecedent soil moisture conditions, the water table depth, and the unsaturated hydrologic properties of the soil.

The recharge rate, the water table depth, and the soil moisture conditions all vary widely across a basin and depend largely on basin topography. With two- and three-dimensional models we can investigate these variations. We can also study the effect of the positioning of infiltration sources on the watershed: their location, their areal extent, and their spacing. Finally we can examine the effect of the three-dimensional configuration of geologic formations and soil types.

The hypothetical basin I have chosen for analysis is shown in Figure 3*a* (at a 2:1 vertical exaggeration). The boundary conditions involve a stream AB at constant hydraulic head, an impermeable basement AFED, and the ground surface BCD on which the hydraulic head, pressure head, or flux regime may be specified. The development of a seepage face above B is allowed.

In all the simulations presented, the initial conditions are those of steady state flow. To determine the steady state configuration, the flux boundary conditions are replaced by specified head values.

The two-dimensional simulations were carried out on a 36 × 48 nodal grid with variable spacings of 10 to 200 cm. The overall dimensions are 3700 cm wide by 700 cm high. The soil type is Del Monte sand [*Liakopoulos*, 1965; *Freeze*, 1969]. This soil has a saturated specific permeability k_0 of 5.8×10^{-9} cm^2 (hydraulic conductivity $K_0 = 1.62$ cm/hr) and a porosity n_0 of 0.30. The compressibility α' was estimated at 3.2×10^{-8} cm^{-1}. The small air entry pressure shown by the original data was ignored so that the $\psi = 0$ water table line would be coincident with the $\theta = 0.30$ line.

One can invoke similitude considerations to extrapolate the results from such a small simulated section to the much larger basins in which we may be interested. The similitude relationships can be derived from the considerations of *Verma and Brutsaert* [1970]

$$\frac{x_1}{x_2} = \frac{y_1}{y_2} = \frac{z_1}{z_2} = \frac{t_1}{t_2} = \frac{\psi_1^*}{\psi_2^*}$$

where ψ_1^* and ψ_2^* are the pressure head values at any θ in the ψ–θ relationship, or at any K in the ψ–K relationship for the basin soil. Extrapolation thus involves an interaction of length unit, time unit, and soil type. The degree of extrapolation is limited by the factor by which the soil moisture curves can be multiplied without giving rise to an unrealistic soil. It is worth noting that the K_0 and n_0 values are not affected by the similitude conversions.

In Figures 3 through 7, the pressure head and total hydraulic head values can be considered to be in cm and the time values in hours for the 3700 × 700 cm basin. For a basin of 3700 × 700 feet with the corresponding soil type (if one exists), the head values would be in feet and the time values in 1.25 days.

A water table rise can result from three types of infiltration events: a rainstorm (broad areal extent, high rate, short duration), a snowmelt type source (broad areal extent, low rate, long duration), and ponding (areally concentrated, high rate, long duration). Figures 3, 4, and 5 show the transient response of a saturated–unsaturated flow system to these three types of hydrologic events.

Figures 3*a*, 3*b*, and 3*c* show the initial steady state flow conditions in the basin when the boundary CD is kept at $\psi = -100$ cm. The pressure head field is the direct numerical solution; the other two fields are deduced from it. The position of the water table can be determined from Figure 3*a*, and its relation to the overlying moisture contents from 3*b*. Figure 3*c* shows the hydraulic head field from which quan-

titative flow nets can be constructed. Owing to the spatial variations of k in the unsaturated zone, the construction of a flow net there is not a trivial exercise.

In Figure 3*d* the transient rise of the water table resulting from a 7-hour rainfall at I_s = 1.5 cm/hr = $0.92K_0$ over the entire basin is shown. There is a 5-hour time lag before the advancing wetting front can induce a water table rise. A comparison of Figures 3*b* and 3*e* shows the dramatic increase in moisture content that occurs throughout the unsaturated portion of the basin. A comparison of Figures 3*c* and 3*f* shows the corresponding increase in the quantity of flow. The formation of a seepage face above the stream provides a discharge area of constantly increasing size. The rapid and significant response of the basin is caused by a shallow water table, wet initial moisture conditions, and a high rainfall rate.

The time lag created by less ideal conditions is shown in Figure 4. Here the initial steady state flow conditions that result from the imposition of a hydraulic head value of 400 cm along CD feature a deep, nearly flat water table and very dry surface moisture conditions. The flux, I_s = 0.15 cm/hr = $0.092K_0$, (Figure 4*d*) is meant to represent a snowmelt type infiltration event. It creates a water table rise that begins after 100 hours and approaches the surface after 400 hours.

Figure 5 shows the effect of areally concentrated infiltration. The initial conditions are the same as those shown in Figure 3. One can imagine the flux rates resulting from surface runoff into depressions during spring snowmelt events similar to the one shown in Figure 4. Once saturation is achieved at the surface, the flux rate boundary condition is replaced by a specified head ponding condition. The water table rise is more rapid at the upstream source because the initial depth to the water table there was less. At the downstream source the moisture content field gives evidence of incipient saturation.

Figures 3, 4, and 5 consider only three cases from an infinite possible selection of surface boundary conditions. We could, for example, consider a storm passage across the basin with its time varying flux values. The chance of

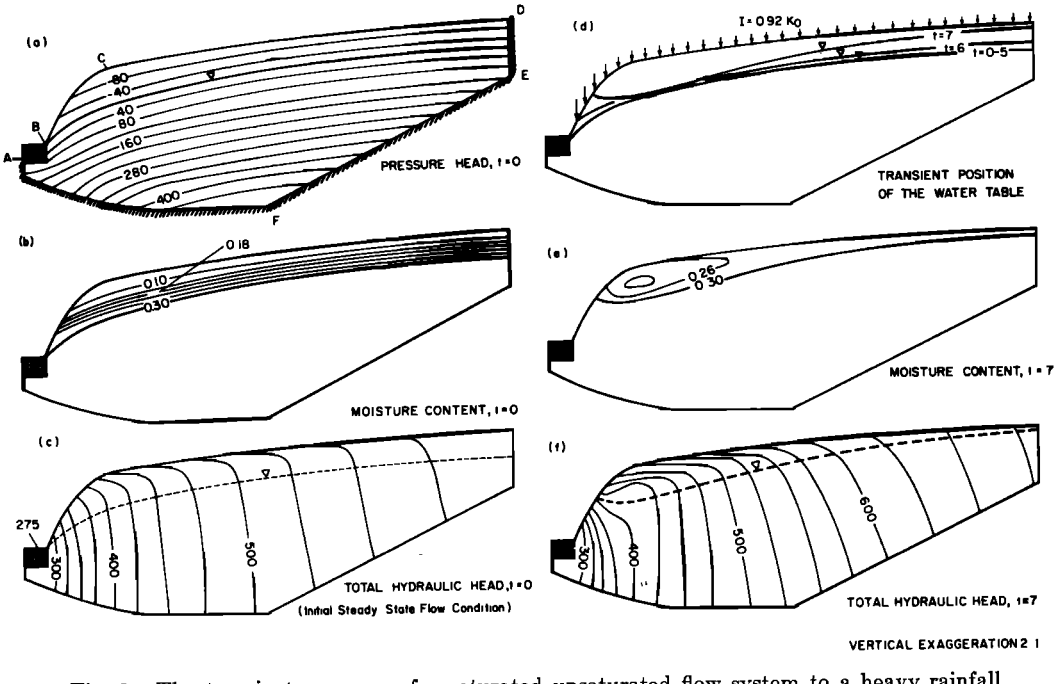

Fig. 3. The transient response of a saturated–unsaturated flow system to a heavy rainfall. (*a*, *b*, *c*) Initial steady state flow conditions. (*d*) Transient water table fluctuation. (*e*, *f*) Final moisture content and total head configurations.

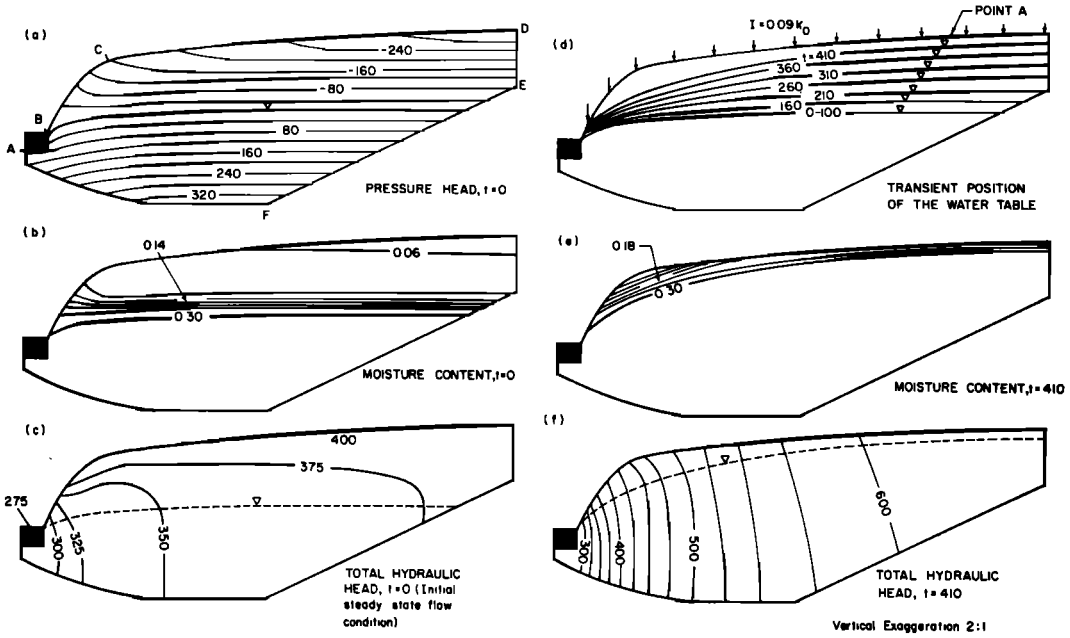

Fig. 4. The transient response of a saturated–unsaturated flow system to snowmelt type infiltration.

arriving at meaningful generalizations from hypothetical models for such systems seems slight, and these are best withheld until the model is applied to real basins and real hydrologic events.

The simulation results can be interpreted quantitatively to give three types of hydrographs. First, the timewise variation in surface infiltration rate can be calculated for any point on the ground surface; second, the water table rise can be charted at any point on the basin; and third, a stream base flow hydrograph can be prepared. Figure 6*a* shows the first two of these hydrographs for point A on Figure 5.

In Figure 6*b*, I have generalized the results of several runs to show schematically the nature of simulated surface infiltration rates. For flux rates greater than the saturated hydraulic conductivity of the soil, surface saturation and ponding occur, and the infiltration rate is reduced to a value that approaches the hydraulic conductivity asymptotically. Another reduction occurs with saturation of the entire profile at that point. The ultimate minimum infiltration rate would equal the rate of groundwater flow at the surface under conditions of a fully saturated basin.

In my earlier one-dimensional treatment [*Freeze*, 1969] the rate of reduction of infiltration rate under ponded conditions was overestimated, owing to an inconsistency in my solution that was brought to my attention by Professor A. J. Sutherland of the University of Canterbury, New Zealand (personal communication, 1970). Under ponded conditions, the ponded pressure head was allowed to propagate down through the profile under the influence of a unit hydraulic gradient that was assumed to have been reached upon ponding. In actual fact, the pressure head profile will show a linear increase from the inverted water table to the ground surface at any time during ponding. As the inverted water table descends, the unit hydraulic gradient will be approached asymptotically. For the cases simulated in the earlier paper, the flaw was not quantitatively significant. In the present study, the solution is completely general, and the correct profile and infiltration rates are obtained for ponded as well as nonponded conditions.

Calculation of the difference between the rainfall rate and the infiltration rate leads to a rainfall excess hydrograph that is of key importance in hydrologic response modeling.

Figure 6*c* shows two generalized water table

fluctuations. The concave recessions are of the form observed in runs simulating redistribution under conditions of no surface evaporation.

PERCHED WATER TABLES

The formation of perched water tables above the main groundwater zone has always been of interest to hydrogeologists. The present model allows investigation of the mechanisms involved. Figure 7*a* shows the introduction of some geologic inhomogeneity to the basin. The clay layer that has been inserted in the unsaturated zone has a saturated permeability 10 times less than the surrounding Del Monte sand and a porosity twice as high. A hypothetical set of unsaturated soil properties was generated by the author.

Figure 7*b* shows the low initial moisture contents at the surface and the nearly flat configuration of the water table. Concentration of vertical flow in the unsaturated zone through the clay layer is shown in Figure 7*c*. There are low gradients, as expected, in the high permeability basal formation. The boundary conditions that give rise to this initial steady state flow system are the same as those for Figure 4.

Under the influence of a broad areal infiltration arising from a flux rate of $I = 0.09K_0$, a perched water table forms above the upper clay layer (Figure 7*d*). It begins as a small lens after 210 hours and builds to a continuous zone after 260 hours. After 460 hours the perched water table has joined with the slowly rising main water table. Increased flow gradients occur throughout the system (Figure 7*f*) but are concentrated in the unsaturated zone.

BASE FLOW

Perhaps the most important hydrograph that

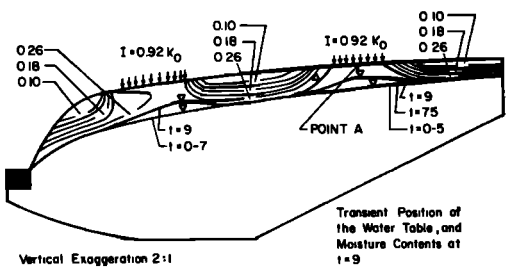

Fig. 5. The transient response of a saturated-unsaturated flow system to areally concentrated infiltration.

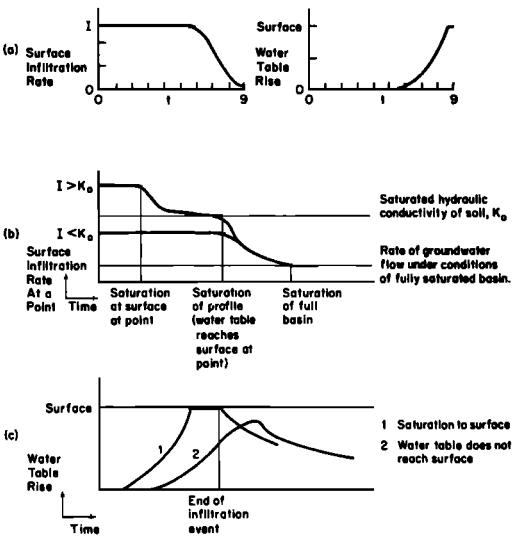

Fig. 6. (*a*) Surface infiltration rate and water table rise at point A in Figure 5. (*b*) Schematic diagram of theoretical infiltration rates. (*c*) Schematic diagram of theoretical water table fluctuations.

can be determined by a basin wide transient analysis is the stream base flow hydrograph. If we define base flow as the amount of water arriving at the stream as saturated flow into the stream bed itself, plus percolation from the seepage face on the stream bank, then we can calculate this quantity from a flow net analysis of the total hydraulic field determined from the mathematical model. We will not consider the effect of flood waves in the stream or the consequent bank storage.

Theoretical base flow curves that are determined from mathematical models but consider only the saturated zone have been presented by *Ibrahim and Brutsaert* [1965] and *Singh* [1968, 1969]. As qualitatively recognized by *Singh* [1968], however, the unsaturated zone plays an important role. A recent paper by *Verma and Brutsaert* [1970] includes the unsaturated zone in a base flow-like application.

The base flow rate at any point in the stream is a consequence of the hydraulic gradient in the vicinity of the stream. Increased base flow results from an increased gradient near the stream, which itself is a consequence of increased up-basin gradients created by a water table rise. The time lag between a surface infiltration event

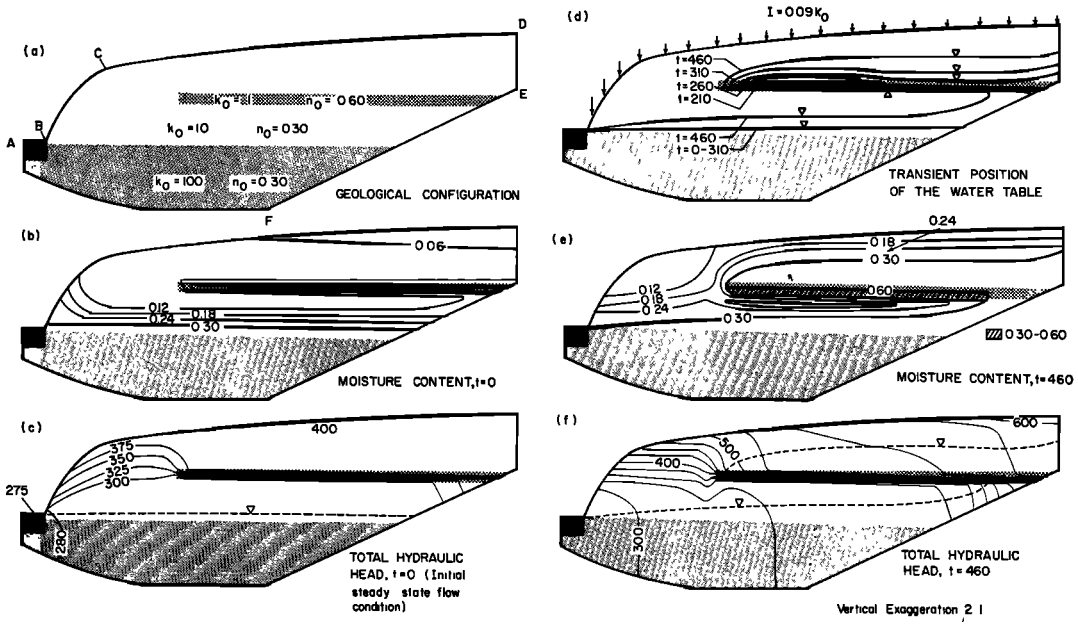

Fig. 7. The formation of a perched water table.

and an increase in stream base flow is therefore directly related to the time required for the infiltration event to induce a widespread water table rise. An example of this direct relationship is shown by Figures 8*a* and 8*b*, taken from the output for Figure 4.

It is easy to calculate two other important base flow quantities. D_{max}, the maximum possible base flow, is the discharge into the stream under conditions of a fully saturated basin. D_{min} is the minimum likely base flow, as calculated under conditions of the lowest recorded water table configuration. Any technique for base flow estimation or base flow separation should consider a curve that lies between D_{min} and D_{max} and is of the form shown in Figure 8*c*, wherein the recession portion of the hydrograph is similar in form to the water table recession curve of Figure 6*c*.

BASIN YIELD

In basin wide water resource evaluation, the most important application of simulation models lies in the prediction of basin response to proposed development. Recent basin wide groundwater simulations have tended to take one of two forms. In the first approach [*Tyson and Weber,* 1964; *Bittinger et al.,* 1967; *Pinder and Bredehoeft,* 1968], transient flow is considered in a two-dimensional horizontal aquifer. This approach is well suited to the prediction of effects of pumpage in a developed basin dominated by a major confined aquifer. It relates the source of the pumped water to the whole of the aquifer and to the leaky overlying beds but does not relate the source of the leakage water to the recharge–discharge properties of the basin.

In the second approach [*Fayers and Sheldon,* 1962; *Tóth,* 1963; *Freeze and Witherspoon,* 1966], steady state flow is considered in two-dimensional, vertical cross sections. This technique is suited to virgin basins or to weakly developed basins and provides a good understanding of the natural recharge–discharge properties of the basin. This approach provides no information on the effects of development. *Bredehoeft and Young* [1970] have pointed out that major groundwater development may significantly change the recharge–discharge regime.

Clearly, the basin yield depends both on the manner in which the effects of withdrawal are transmitted through the aquifers and on the changes in rates of groundwater recharge and discharge induced by the withdrawals. To

analyze these latter effects, one must include the unsaturated zone in the three-dimensional transient analysis. With the present model we can analyze the effects, regardless of whether the wells are finished in confined or unconfined aquifers. The response will, of course, be dependent on the number of wells, their areal position, and the rates of pumpage.

To illustrate these effects on basin yield, I have designed a simple hypothetical three-dimensional basin whose essential features are shown in Figure 9*a*. It is a rectangular subbasin with uniform flow from right to left under initial steady state regional flow conditions. Inflow to the basin is restricted to the upstream portion of the ground surface (above WXYZ in the plan view, along CD in the vertical section). For the initial steady state calculations the pressure head was kept constant at −20 cm in this area; during the transient run an influx value of 0.018 cm/hr ($0.011K_0$) was allowed. Outflow occurs as base flow to a stream at E, kept at constant hydraulic head with the pressure head equal to zero on its surface. All other boundaries are impermeable. The initial location of the water table leaves an unsaturated zone thickening to the left across the basin.

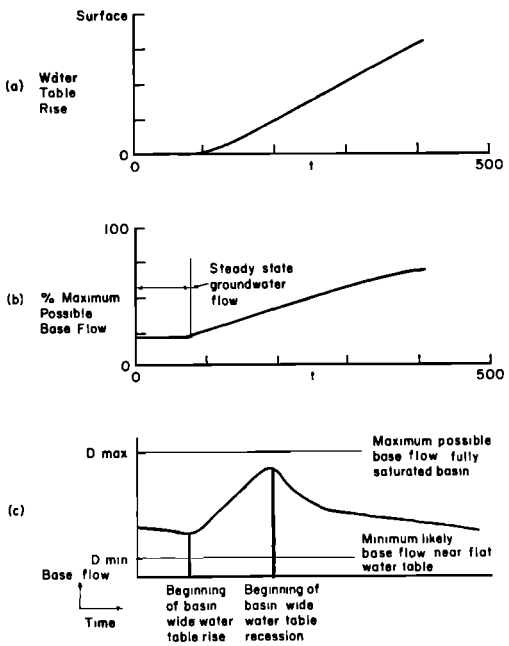

Fig. 8. (*a*) Water table rise at point A in Figure 4. (*b*) Base flow to stream in Figure 4. (*c*) Schematic diagram of theoretical base flow hydrograph.

Geologically, the basin is a two-layer model, the lower layer having a saturated permeability 10 times that of the Del Monte sand in the upper layer. A single well is located just below the upper surface of the lower layer. Thus the model is classically neither confined nor unconfined.

The simulation was carried out on a 26 × 13 × 26 variably spaced grid representing a basin of 5300 × 4000 × 600 cm. Groundwater velocities at the boundaries of the 50 × 50 × 50 cm nodal cube that represented the well site were set at 36 cm/hr, simulating a pumping rate of 540 l/hr (2.4 gpm). In the three-dimensional model, as in the two-dimensional models, similitude can be invoked to apply the results to larger basins. The maximum multiplicative factor is limited in this case by the necessity of maintaining realistic pumping rates.

Figure 9*b* shows two cross sections through the three-dimensional hydraulic head field after 47 hours of pumping. Both the vertical section and the plan are in the plane of the well. If we compare the vertical sections of Figures 9*a* and 9*b*, we can note the following:

1. The hydraulic head has been lowered at almost every point in the basin. The influence of the well has thus been recorded by changes in the piezometric surface throughout the lower aquifer.

2. There has been a drawdown in the water table in the upstream portion of the flow system, which is due in part to the well withdrawals and in part to reduced natural influx rates. (The $I = 0.011\ K_0$ rate is about half the rate that was being accepted under steady state flow conditions.)

3. The gradients in the vicinity of the stream have been reduced and the discharge from the basin by base flow thereby lessened. (Note that the 400 and 450 contours have been displaced to the right.)

4. Groundwater recharge rates at the water table have been maintained in the upstream portion of the system and have increased above the well site, but only at the expense of a falling water table.

Several areas have been outlined on the plan view (Figure 9*b*). The parabolic area LMN

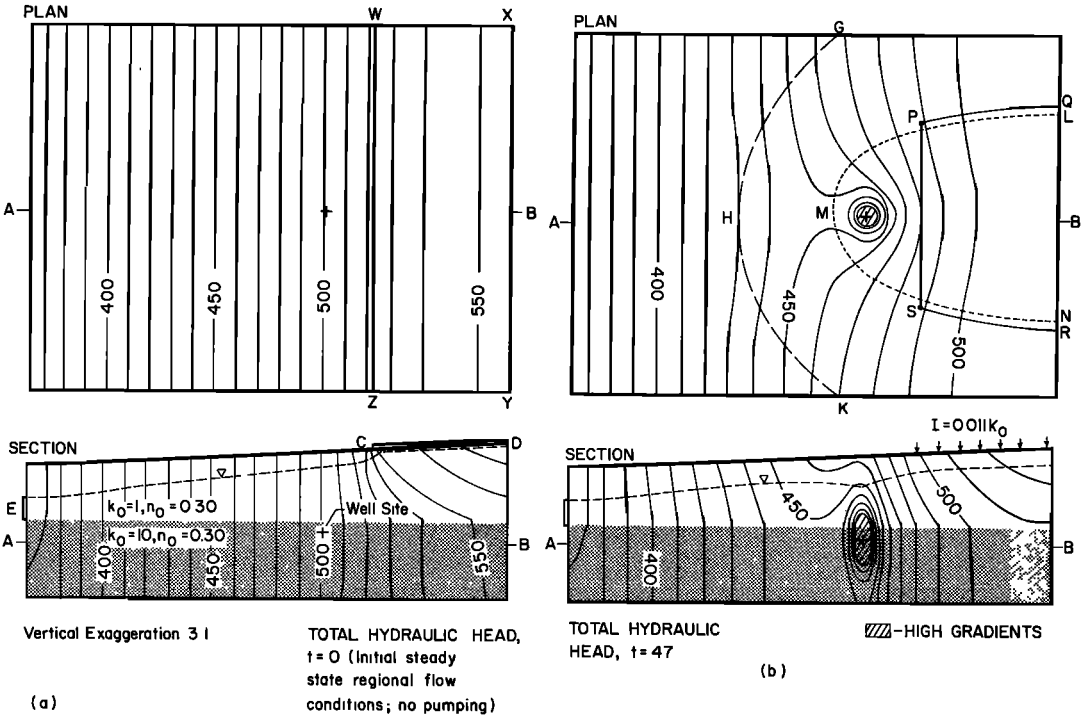

Fig. 9. Transient response of a three-dimensional saturated–unsaturated flow system in a two-layer basin to groundwater withdrawal from a single well.

is that portion of the aquifer inside which flow is contributing to the well. Flow lines originating outside LMN feed stream base flow. LMN is actually the planar intersection of a three-dimensional paraboloid that extends to the ground surface. Its intersection with the ground surface in that area where infiltration occurs is shown by PQRS. The paraboloid of well influence, like the proportion of the total infiltration ultimately captured by the well, is constantly expanding with time.

The area to the right of the GHK line in Figure 9*b* is that area in which the water table has declined. It is interesting to note that the water table has been lowered even in portions of the flow system outside that part directly contributing to the well.

For the case shown in Figure 9, the pumping rate was greater than the total basin infiltration rate by a factor of 3.65. This situation is clearly unstable. If the pumping rate were less than or equal to the influx, an equilibrium steady state flow system not unlike that shown in Figure 9 would result. Figure 10 shows the ultimate result of a basin pumping rate that exceeds the available surface influx but only by a small factor. Here the pumping rate was slightly greater than that in Figure 9, but infiltration was allowed over the entire surface. The hydraulic head pattern shows groundwater withdrawals in equilibrium with increased natural infiltration rates and induced recharge from the stream.

Figures 9 and 10 assume constant low rate infiltration at the surface over long periods of time. The actual transient nature of the surface boundary conditions exerts great influence on the basin response. It is unlikely, for example, that a flow system like that shown in Figure 10 could exist in a large basin. The water table depths would be too great for the unsaturated flow processes to deliver the recharge rate on a sustained basis. As the water table drops, the likelihood of infiltration being recaptured by evaporation during the redistribution period becomes greater.

We can generalize the insights gained from the three-dimensional hypothetical examples by

considering schematically the response of a basin to increased development. If we isolate the saturated portion of the basin and integrate the spatially varied recharge and discharge rates to obtain basin wide totals for any given time period, then the response to withdrawal at a rate Q can be described by [*Bredehoeft and Young*, 1970]

$$Q = R - D + \frac{dS_s}{dt} \qquad (14)$$

where R is the basin wide total recharge rate; D, the basin wide total discharge rate, is equal to $D_s + D_u$, D_s being the saturated discharge rate (principally base flow) and D_u the discharge to the unsaturated zone; and dS_s/dt is the change of storage in the saturated zone.

The recharge rate R is dependent on conditions in the unsaturated zone

$$R = I + D_u - E + \frac{dS_u}{dt} \qquad (15)$$

where I is the basin wide total surface infiltration rate, E is the basin wide total surface exfiltration rate, under the influence of evapotranspiration, and dS_u/d_t is the change in storage in the unsaturated zone.

If we increase the withdrawal rate with time (that is, if $Q = Q(t)$), then all the dependent parameters in equations 14 and 15 also become time dependent; in particular, $R = R(t)$ and $D = D(t)$. The key to understanding the dynamic response of a groundwater basin and to determining its yield lies in predicting the changes in $R(t)$ and $D(t)$ that result from changes in $Q(t)$.

As has been emphasized in this paper, the flow rates at the water table $R(t)$ and $D(t)$ are functions of time not only under the influence of $Q(t)$ but also under the influence of the natural transient climatic boundary conditions at the ground surface. The mechanism by which the unsaturated zone attenuates the influence of transient climatic conditions on the rate of flow that actually arrives at the water table to sustain the groundwater flow pattern is treated by *Freeze* [1969]. The average annual recharge rate may be a high or low percentage of the total annual precipitation. The recharge rate is dependent on the rates and durations of rainfalls (particularly whether the rainfall rates are greater or less than the saturated permeability) and on subsequent climatic conditions at the surface during redistribution periods. The rate is highly dependent on the depth to the water table.

I will now present two schematic diagrams (Figures 11*a* and 11*b*) that represent conditions in a groundwater basin under increased development. I apologize for the obtuseness that attends their explanation, but I can find no simpler words. The diagrams concern flux rates in the saturated zone alone. To simplify the analysis further, it is assumed that the attenu-

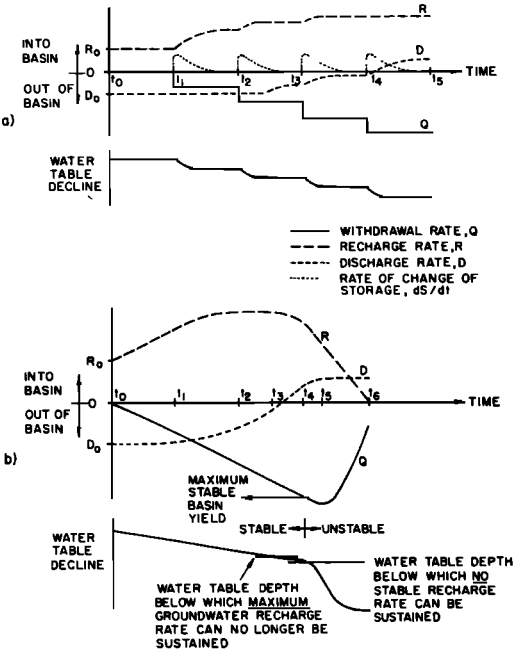

Fig. 11. Schematic diagram of transient relationships between recharge rates, discharge rates, and withdrawal rates.

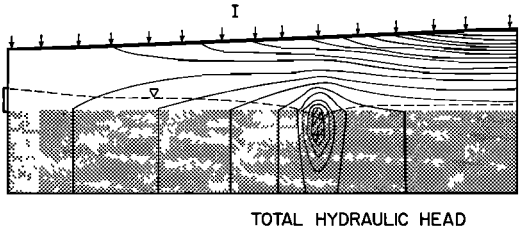

Fig. 10. Groundwater withdrawal in equilibrium with increased natural recharge rates and induced recharge from stream.

ating effect of the unsaturated zone has been complete and that natural variations in R and D are far less than those caused by changes in Q.

In Figure 11*a* (at time t_0) under virgin conditions, we have a basin wide total recharge rate R_0 equal to the basin wide total discharge rate D_0. (In earlier papers, the author has referred to this quantity as the natural basin yield.) If at time t_1 we begin pumping at a rate Q, the withdrawals are initially balanced by a change in storage, which in an unconfined aquifer takes the form of an immediate water table decline. At the same time, the basin strives to set up a new equilibrium under conditions of increased recharge R. The unsaturated zone will now be induced to deliver greater flow rates under the influence of the higher gradients in the saturated zone. If increased withdrawals occur at time t_2, there is again a change in storage pulse, a lowered water table, an increased recharge rate R, and perhaps a decreased discharge rate D.

In the simplified case shown in Figure 11*a*, steady state equilibrium conditions are reached prior to each new increase in withdrawal rate. We might consider the diagram to represent the addition of single wells to a small basin at widely spaced time intervals over a period of several years. Just after time t_4, all natural discharge ceases, and the discharge curve D rises above the horizontal axis, implying the presence of induced recharge from a stream that had previously been accepting base flow. The withdrawal Q is now fed by the regional recharge rate R and the induced recharge rate D. Note that the regional recharge rate R attained a maximum between times t_3 and t_4. At this rate, the groundwater body is accepting all the infiltration that is available from the unsaturated zone under the lowered water table conditions.

In Figure 11*a* the increases in withdrawal rate did not lead to undesired effects. The pertinent question in water resource planning is, How can we maximize the basin yield without causing unacceptable water table declines or significant reductions in the natural replenishment of the basin? In Figure 11*b*, I present one possible form of analysis. It is basically a generalized form of Figure 11*a*.

The time scale is in years, and the figure purports to trace schematically the basin wide total rates of recharge R and discharge D and the decline of the water table under conditions of constantly increasing groundwater development. The sequence of events shown in Figure 11*b* may differ in their order from basin to basin or within the same basin under different developmental proposals. For development of confined aquifers there will be a significant time lag before water table declines manifest themselves, but sooner or later they must occur.

In Figure 11*b* at time t_0, natural steady state flow conditions prevail. As the withdrawal rate Q increases, the water table declines, and there is an induced increase in the regional recharge rate R. The regional discharge rate D remains constant until t_1, when discharge out of the basin begins to lessen and thus allows a lower rate of increase in the recharge rate R while maintaining an increased withdrawal rate Q. At time t_2, the maximum available recharge rate R is reached. The increasing Q rates must now be fed by more rapidly decreasing discharge rates D; the result is a crossover of the D curve shortly after t_3, which signifies the beginning of induced recharge conditions. At time t_3, however, the declining water table reaches a depth below which the maximum rate of groundwater recharge R can no longer be sustained. The same annual precipitation rate no longer provides the same percentage of infiltration to the water table owing to the consistently drier conditions in the unsaturated zone [*Freeze*, 1969]. Evapotranspiration during redistribution now takes more of the infiltrated rainfall before it has a chance to percolate down toward the groundwater zone.

The decreased regional recharge rate R between t_3 and t_4 (Figure 11*b*) is made up for by an increased induced recharge rate D. At t_4 the water table reaches a depth below which no stable recharge rate can be sustained; at t_5 the maximum available rate of induced recharge is attained. From time t_5 it is impossible for the basin to supply increased rates of withdrawal. The only source lies in an increased rate of change of storage that manifests itself in rapidly declining water tables. By time t_6 the water table has been lowered to a nearly flat configuration connecting the well depth to the stream. The total source of withdrawal Q now comes from induced recharge D.

During time t_4 to t_6 the basin yield has become unstable. The value of Q at time t_4 represents the maximum stable basin yield. The maximum stable yield could theoretically be maintained indefinitely, since the water table depth is still high enough for the unsaturated zone to deliver a sustained annual groundwater recharge rate. To develop a basin to its limit of stability would, of course, be foolhardy. A dry year might cause an irrecoverable water table drop. The basin safe yield must allow for a factor of safety and is therefore somewhat less than the maximum stable basin yield.

This discussion of basin yield, although carried out with a schematic diagram based on results from a hypothetical model, is not academic. Each quantity in Figure 11*b*, and its variation over space and time, can be predicted, within the limitations of the technique, by a three-dimensional, transient, saturated–unsaturated basin model.

CONCLUSIONS

1. It is possible to simulate transient subsurface flow in a three-dimensional, heterogeneous, anistotropic, saturated–unsaturated, confined–unconfined geologic basin. The equation of flow is a combination of the Jacob–Cooper equation for saturated flow and the Richards equation for unsaturated flow. The equations can be solved by the line successive overrelaxation technique with a program that allows for a variable grid and any generalized region shape. At any boundary node, time variant boundary conditions can be imposed that specify the head, the flux, or no-flow conditions. Groundwater withdrawals can be represented by an internal source or sink of specified head or flux. Input parameters include the surface flux rates due to rainfall, evaporation, or ponding, and the soil and formation properties. Among the soil and formation properties are directional permeabilities, compressibility factors, and hysteretic relationships between unsaturated permeability, moisture content, and moisture tension. Output is in the form of plots of the pressure head, total head, and moisture content fields for any cross section at any time step. From the output it is possible to develop quantitative hydrographs of surface infiltration, groundwater recharge, water table depth, and stream base flow.

2. Simulations of natural flow systems in hypothetical basins provide insight into the mechanisms involved in the development of perched water tables and in the areal variation of water table fluctuations. The time lag between a surface infiltration event and an increase in stream base flow is directly related to the time required for the infiltration event to induce a widespread water table rise.

3. The inclusion of the unsaturated zone in the analysis enables one to make a complete analysis of the basin yield under developed conditions. One can simulate not only the manner in which the effects of withdrawal are transmitted through the aquifers but also the changes in the rates of groundwater recharge and discharge induced by the withdrawals. For any proposed developmental scheme, one can predict the maximum basin withdrawal that can be sustained in the long term by a flow system in equilibrium with the recharge–discharge characteristics of the basin.

4. Three critical assumptions in the mathematical development disallow consideration of entrapped air, swelling soils, or the effect of temperature gradients. These restrictions may limit the value of the present model for direct use in overall watershed response models. Computer limitations restrict the size of basins that can be modeled to a few square miles by 1000 feet deep.

NOTATION

$x, y, z,$ coordinate directions, cm;
$z,$ elevation head, cm of water;
$\psi,$ pressure head, cm of water;
$\phi,$ total hydraulic head, cm of water;
$g,$ acceleration due to gravity, cm/sec^2;
$\mu,$ viscosity of water, gm/cm sec;
$\rho,$ density of water, gm/cm^3;
$k,$ specific permeability, cm^2;
$K,$ hydraulic conductivity, cm/sec;
$n,$ porosity, decimal fraction;
$\theta,$ moisture content, decimal fraction;
$S,$ fractional saturation, decimal fraction;
$C,$ specific moisture capacity, cm^{-1} of water;
$\alpha',$ vertical compressibility of formation, cm^{-1} of water;
$\beta',$ compressibility of water, cm^{-1} of water;
$t,$ time, sec;
$\Delta x, \Delta y, \Delta z,$ nodal spacings, cm;
$\Delta t,$ time step, sec;

ψ_I–ψ_{VI}, predicted pressure heads at nodal boundaries;
ψ_{VII}, predicted pressure head at node center;
ω, overrelaxation parameter;
λ, prediction parameter;
I_x, I_y, I_z, flux rates, cm/sec;
i, j, k (subscripts), nodal number in x, y, z directions;
t, it (superscripts), time step number, iteration number;
0 (subscript), at saturation (e.g., k_0, K_0, n_0).

REFERENCES

Bittinger, M. W., H. R. Duke, and R. A. Longenbaugh, Mathematical models for better aquifer management, 15 pp., Symposium on artificial recharge and management of aquifers, International Association of Scientific Hydrology, Haifa, Israel, 1967.

Bjordammen, J., and K. H. Coats, Comparison of alternating direction and successive overrelaxation techniques in simulation of reservoir fluid flow, *Soc. Petrol. Eng. J., 9,* 47–58, 1969.

Bredehoeft, J. D., and R. A. Young, The temporal allocation of ground water—A simulation approach, *Water Resour. Res., 6*(1), 3–21, 1970.

Briggs, J. E., and T. N. Dixon, Some practical considerations in the numerical solution of two-dimensional reservoir problems, *Soc. Petrol. Eng. J., 8,* 185–194, 1968.

Cooley, R. L., A finite-difference method for analyzing liquid flow in variably saturated porous media, 37 pp., *Hydrol. Eng. Center Tech. Pap. 22,* U.S. Army Corps of Engineers, Sacramento, California, 1970.

Cooper, H. H., Jr., The equation of groundwater flow in fixed and deforming coordinates, *J. Geophys. Res., 71*(20), 4785–4790, 1966.

Dorsey, N. E., *Properties of Ordinary Water-Substance,* 673 pp., Reinhold, New York, 1940.

Douglas, J., Jr., and H. H. Rachford, Jr., On the numerical solution of heat conduction problems in two and three space variables, *Trans. Amer. Math. Soc., 82,* 421–439, 1956.

Fayers, F. J., and J. W. Sheldon, The use of a high speed digital computer in the study of the hydrodynamics of geologic basins, *J. Geophys. Res., 67*(6), 2421–2431, 1962.

Freeze, R. A., The mechanism of natural groundwater recharge and discharge, 1, One-dimensional, vertical, unsteady, unsaturated flow above a recharging or discharging ground-water flow system, *Water Resour. Res., 5*(1), 153–171, 1969.

Freeze, R. A., and R. L. Harlan, Blueprint for a physically-based, digitally-simulated hydrologic response model, *J. Hydrol., 9,* 237–258, 1969.

Freeze, R. A., and P. A. Witherspoon, Theoretical analysis of regional groundwater flow, 1. Analytical and numerical solutions to the mathematical model, *Water Resour. Res., 2*(4), 641–656, 1966.

Green, D. W., H. Dabiri, C. F. Weinaug, and R. Prill, Numerical modeling of unsaturated groundwater flow and comparison of the model to a field experiment, *Water Resour. Res., 6*(3), 862–874, 1970.

Hornberger, G. M., I. Remson, and A. A. Fungaroli, Numeric studies of a composite soil moisture ground-water system, *Water Resour. Res., 5*(4), 797–802, 1969.

Ibrahim, H. A., and W. Brutsaert, Inflow hydrographs from large unconfined aquifers, *J. Irrig. Drain Div., Amer. Soc. Civil Eng., 91*(IR2), 21–38, 1965.

Jacob, C. E., The flow of water in an elastic artesian aquifer, *Trans. Amer. Geophys. Union,* part 2, 574–586, 1940.

Jeppson, R. W., Numerical solution of the steady-state two-dimensional flow system resulting from infiltration on a watershed, 39 pp., *Water Res. Lab. Rep. PRWG-59c-1,* Utah State University, Logan, 1969.

Liakopoulos, A. C., Retention and distribution of moisture in soils after infiltration has ceased, *Bull. Int. Ass. Sci. Hydrol., 10,* 58–69, 1965.

Madsen, O. S., A note on the equation of groundwater flow, *Water Resour. Res., 5*(5), 1157–1158, 1969.

Nelson, R. W., Flow in heterogeneous porous mediums, 1. Darcian-type description of two-phase systems, *Water Resour. Res., 2*(3), 487–495, 1966.

Pinder, G. F., and J. D. Bredehoeft, Application of the digital computer for aquifer evaluation, *Water Resour. Res., 4*(5), 1069–1093, 1968.

Richards, L. A., Capillary conduction of liquids through porous mediums, *Physics, 1,* 318–333, 1931.

Rubin, J., Theoretical analysis of two-dimensional, transient flow of water in unsaturated and partly unsaturated soils, *Soil Sci. Soc. Amer. Proc., 32,* 607–615, 1968.

Singh, K. P., Some factors affecting baseflow, *Water Resour. Res., 4*(5), 985–999, 1968.

Singh, K. P., Theoretical baseflow curves, *J. Hydraul. Div., Amer. Soc. Civil Eng., 95*(HY6), 2029–2048, 1969.

Stone, H. L., Iterative solution of implicit approximations of multidimensional partial differential equations, *J. Soc. Ind. Appl. Math., J. Numer. Anal., 5,* 530–558, 1968.

Taylor, G. S., and J. N. Luthin, Computer methods for transient analysis of water-table aquifers, *Water Resour. Res., 5*(1), 144–152, 1969.

Tóth, J., A theoretical analysis of groundwater flow in small drainage basins, *J. Geophys. Res., 68*(16), 4795–4812, 1963.

Tyson, H. N., Jr., and E. M. Weber, Computer simulation of groundwater basins, *J. Hydraul. Div., Amer. Soc. Civil Eng., 90*(HY4), 59–77, 1964.

Verma, R. D., and W. Brutsaert, Unconfined aquifer seepage by capillary flow theory, *J. Hydraul. Div., Amer. Soc. Civil Eng., 96*(HY6), 1331–1344, 1970.

Verruijt, A., Elastic storage of aquifers, in *Flow Through Porous Media,* edited by R. J. M. De Wiest, pp. 331–376, Academic, New York, 1969.

Wachpress, E. L., and G. J. Habetler, An alternating-direction-implicit iteration technique, *J. Soc. Ind. Appl. Math., 8,* 403, 1960.

Weinstein, H. G., H. L. Stone, and T. V. Kwan, Iterative procedure for solution of systems of parabolic and elliptic equations in three dimensions, *Ind. Eng. Chem. Fundam., 8,* 281–287, 1969.

Young, D. M., Jr., The numerical solution of elliptic and parabolic partial differential equations, in *Survey of Numerical Analysis,* edited by J. Todd, pp. 380-438, McGraw-Hill, New York, 1962.

(Manuscript received October 19, 1970;
revised December 22, 1970.)